ARTICLE

# Stability of the Two Au−S Binding Modes in $Au_{25}(SG)_{18}$ Nanoclusters Probed by NMR and Optical Spectroscopy

**Zhikun Wu and Rongchao Jin***

Department of Chemistry, Carnegie Mellon University, Pittsburgh, Pennsylvania 15213

**ABSTRACT** This report presents a detailed investigation on the structural stability of the $Au_{25}(SG)_{18}$ nanoclusters (where, −SG represents glutathionate) with a focus on the oxidation resistance and thermal stability of the Au−S bonds in the cluster. Two types of Au−S binding modes were previously indentified in the crystal structure of phenylethylthiolate-capped $Au_{25}$ clusters, and the $Au_{25}(SG)_{18}$ nanoclusters have been confirmed to adopt the same structure as $Au_{25}(SCH_2CH_2Ph)_{18}$ in our previous works. Herein, NMR in combination with optical spectroscopy revealed some distinct differences in both antioxidation and thermal stability of the two Au−S binding modes in the $Au_{25}(SG)_{18}$ nanocluster, that is, the mode I thiolate ligands (total 12 ligands) exhibit a much higher stability than the mode II ligands (total 6 ligands). Upon the basis of this major observation as well as an abundant $[Au_{25}S_{12}]^-$ species detected in laser desorption ionization (LDI) mass spectrometry analysis of $Au_{25}(SG)_{18}$ clusters, a metastable species similar to $Au_{25}(SG)_{12}$ (*i.e.*, a loss of six type II ligands of −SG) may exist in the processes of oxidation and thermal treatment. Overall, this work provides a deep insight into the intriguing structure of thiolate-capped $Au_{25}$ clusters, which will benefit future studies pertaining to the potential applications of such nanoclusters.

**KEYWORDS:** gold cluster · stability · NMR · Au−S binding

Gold nanoclusters have attracted particular research interest in recent years owing to their interesting optical properties,[1−3] intrinsic magnetism for specific size and charge state,[4] structural transition in gas phase clusters,[5] enhanced luminescence,[6−13] redox properties,[14−20] as well as potential applications in many fields such as catalysis,[21−24] optics,[25−27] sensing,[28−30] and biomedicine.[31,32] The significant advances in nanochemistry have permitted the synthesis of atomically monodisperse gold nanoclusters ($Au_n$, $n$ ranging from a dozen to about a hundred, typically <2 nm).[33−45] These nanoclusters possess a well-defined metal core with a specific number of metal atoms ($n$) and a monolayer ligand shell with a precisely controlled number of protecting ligands. Such nanoclusters provide a unique model system for in-depth investigation of their physical and chemical properties since the heterogeneity of nanoparticles is not present in such systems.

Among the well-defined gold nanoclusters, thiolate-protected $Au_{25}(SR)_{18}$ nanoclusters have been extensively studied.[46−49] Tsukuda *et al.* reported the particular stability of glutathione-capped $Au_{25}(SG)_{18}$.[50] We have previously reported the synthesis of atomically monodisperse $Au_{25}(SCH_2CH_2Ph)_{18}$ nanoclusters through a kinetic control approach,[49] as well as $Au_{25}(SR)_{18}$ functionalized with other types of thiolates, including 11-mercapto-1-undecanolate, glutathionate, hexylthiolate, and dodecylthiolates, *etc.*[51,52] Among them, the $Au_{25}(SCH_2CH_2Ph)_{18}$ nanocluster's crystal structures of their anionic and charge neutral forms have been determined by us;[1,53] note that the anionic structure was also independently reported by Murray and coworkers,[54] and the theoretical structure of $Au_{25}(SCH_3)_{18}^q$ was described by Akola *et al.*[55] For $Au_{25}$ clusters capped by other types of thiolates, we have confirmed, by means of nuclear magnetic resonance (NMR) in conjunction with laser desorption ionization mass spectroscopy (LDI-MS) and other characterization, that $Au_{25}(SR)_{18}$ nanoclusters (where SR = glutathionate, hexylthiolate, and dodecanethiolate) indeed adopt the same structure as $Au_{25}(SCH_2CH_2Ph)_{18}$,[52] that is, the $Au_{25}$ nanocluster features a centered icosahedral $Au_{13}$ kernel (Scheme 1A), which is further encapsulated by an exterior gold shell composed of the remaining 12 gold atoms, hence, a two-shell structure that can be dissected into $Au_{1(center)}/Au_{12(shell\ 1)}/Au_{12(shell\ 2)}$. By taking into consideration of the 18 thiolate ligands, the exterior $Au_{12}$ shell can be viewed as six −S−Au−S−Au−S− staples, which bond to and pro-

*Address correspondence to rongchao@andrew.cmu.edu.

Received for review May 14, 2009 and accepted June 09, 2009.

**Published online June 23, 2009.** 10.1021/nn9004999 CCC: $40.75

tect the $Au_{13}$ kernel (Scheme 1A,B). The $Au_{25}(SR)_{18}$ particle is quite unique in that, except the central gold atom in the icosahedron, all of the 24 gold atoms in the two shells are bonded to thiolates. In terms of their chemical environments, two types of thiolate binding modes are identified: (i) the 12 −SR ligands that join $Au_{12}$ shells 1 and 2 (for the convenience of discussions below, this triangular binding mode is designated as mode I, Scheme 1B); (ii) the six −SR ligands located at the $Au_{12}$ shell 2 (this V-shaped binding mode is designated as mode II, Scheme 1B).

Given the two-shell structure of $Au_{25}(SR)_{18}$ particles and the two binding modes of surface thiolates, some interesting questions naturally arise: (1) Is there any difference in the stability of the two Au−S binding modes? If so, which one is more stable? (2) Are there any stable intermediates if the Au−S bonds are attacked, for example, by oxidants? Answering these questions is particularly important for understanding the structure−property correlation of the $Au_{25}$ nanoclusters as well as for practical applications of such nanoclusters in catalysis and optics. In this work, we employ NMR and optical spectroscopy to investigate the oxidation and thermal stabilities of glutathionate-capped $Au_{25}(SG)_{18}$ nanoclusters. Our results clearly show distinct stability differences between the two types of Au−S binding modes in terms of their oxidation resistance and thermal stability. These results are important for gaining a deep insight into the ligand stability and understanding the intriguing structure of $Au_{25}(SR)_{18}$ nanoclusters.

## RESULTS AND DISCUSSION

The glutathione-capped $Au_{25}(SG)_{18}$ nanoparticles were made *via* a previously reported approach (see Experimental Section for details).[51,52] Herein, we focus on the investigation of their oxidation and thermal stabilities of such nanoclusters. In the oxidation experiment, $Au_{25}(SG)_{18}$ (4.0 mg, 0.38 μmol) was dissolved in 0.4 mL of $D_2O$ in a NMR tube and a spectrum was taken (as the start). Then, cerium(IV) sulfate $Ce(SO_4)_2$ (1.5 mg, 4.5 μmol) was slowly added to the ice-cold solution, and the solution was monitored by NMR as a function of reaction time. Note that $Ce(SO_4)_2$, rather than $H_2O_2$, was used in the oxidation experiment because $Ce(SO_4)_2$ does not interfere with NMR signals, while $H_2O_2$ does; in addition, one can easily control the amount of $Ce(SO_4)_2$, but $H_2O_2$ tends to self-decompose over a long reaction time (*e.g.*, a few days in this work). Nevertheless, the overall oxidation processes involving $Ce(SO_4)_2$ or $H_2O_2$ are similar.

Prior to the addition of oxidants, the NMR spectrum of $Au_{25}(SG)_{18}$ nanoclusters shows broad peaks in the range of 2−4.2 ppm (Figure 1, spectrum a). In our previous work,[52] we have fully assigned the NMR peaks of −SG ligands with the aid of two-dimensional NMR correlation spectroscopy (see labels in Figure 1); note that the 6-C**H** signal is merged with the broad water peak at 4.8 ppm[52] (beyond the range shown in Figure 1). Of particular importance to this work are the NMR signals of the α-H (relative to S atom, labeled as 7; see inset of Figure 1); signal splittings were observed: a doublet at 3.6 and 3.8 ppm (overlapped with 2-C**H**) corresponds to α-H for the triangular Au−thiolate binding mode (I), and another doublet at 3.3 and 3.4 ppm corresponds to α-H for the V-shaped Au−thiolate binding mode (II). Note that the splitting in the doublet is caused by the chirality of the ligands.[52] The triangular mode I thiolates join the $Au_{13}$ kernel and the exterior $Au_{12}$ shell (total 12 such −SR ligands, Scheme 1B), while the V-shaped mode II ligands locate at the exterior $Au_{12}$ shell (total six such ligands, Scheme

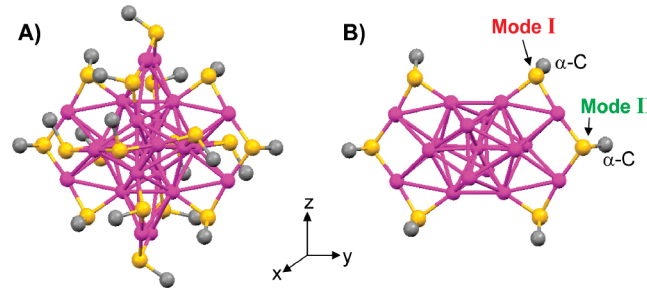


**Scheme 1. Structure of thiolate-protected $Au_{25}(SR)_{18}$ nanoclusters (Au, purple; S, yellow; α-C of thiolate ligands, gray). A portion of the structure is shown in (B), in which two types of thiolates are labeled as I and II.**

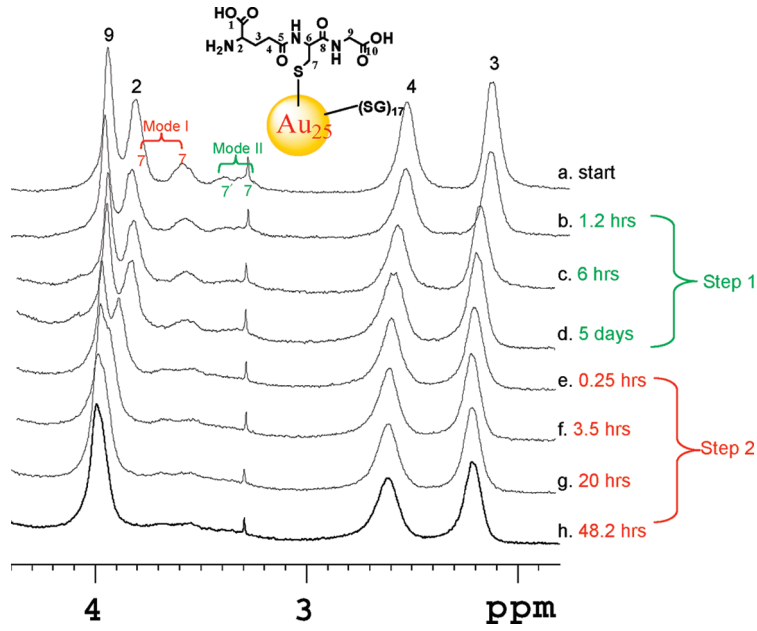


**Figure 1. Time-dependent NMR spectra of $Au_{25}(SG)_{18}$ (in $D_2O$) over the course of oxidation by $Ce(SO_4)_2$: (b−d) after adding 1.5 mg of $Ce(SO_4)_2$ (step 1) and (e−h) after adding additional 1.5 mg of $Ce(SO_4)_2$ (step 2). The *sharp* peak at 3.3 ppm residing on a broad peak (assigned to 7′-$CH_2$ of thiolates) arises from residual $CH_3OH$ in the sample.**

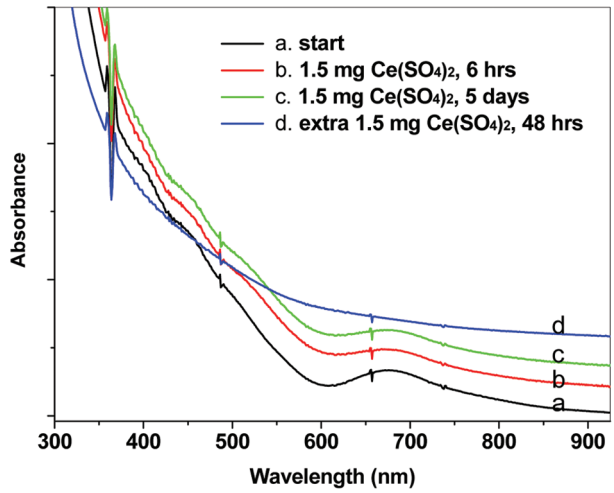


**Figure 2. UV−vis absorption spectra of $Au_{25}(SG)_{18}$ (in $D_2O$) after the addition of $Ce(SO_4)_2$ in steps 1 and 2, respectively. The spectra are shifted for the ease of comparison.**

1B). The ratio of mode I (downfield in NMR) to II (upfield) is 2:1. Note that the sharp peak residing on the broad signal at 3.3 ppm arises from residual MeOH present in the $Au_{25}(SG)_{18}$ sample, but it does not affect our spectral analysis.

After the addition of $Ce(SO_4)_2$, the doublet at 3.3/3.4 ppm became broadened and eventually hardly observable after 6 h (spectra a−c, Figure 1). This indicates that the thiolates of model II were first attacked by the oxidant, and the gold−thiolate linkages and accordingly the NMR signals were affected. In contrast, the doublet at 3.6/3.8 ppm, which corresponds to the ligands in the Au−S binding mode I, is not affected even after 5 days (Figure 1, spectrum d) and their signals are almost identical to the starting 3.6/3.8 ppm doublet. This indicates the particular stability of the mode I thiolates.

The extraordinary oxidation resistance of mode I thiolates compared with that of mode II thiolates is also indicated by UV−vis spectroscopic measurements (Figure 2). After the oxidation for 5 days (longer time was not investigated), no changes were found in the absorption spectra (Figure 2). Note that the $Au_{25}$ structure consists of a $Au_{13}$ kernel and an exterior shell of 12 gold atoms (Scheme 1). The optical properties of $Au_{25}(SG)_{18}$ are primarily contributed by the $Au_{13}$ kernel;[1,56] The six mode II thiolates exclusively bind to the exterior gold shell and do not significantly contribute to the optical absorption peaks, thus, even when these ligands were attacked in the first step of oxidation (1.5 mg of $Ce(SO_4)_2$ added), no apparent changes in the UV−vis spectrum were observed. The close resemblance of the optical spectrum to the starting spectrum indicates that the $Au_{25}$ frame structure should be preserved during the oxidation reaction (step 1).

Interestingly, after addition of an additional amount of $Ce(SO_4)_2$ (1.5 mg, 4.5 μmol, step 2, Figure 1), the mode I ligands can no longer resist oxidation and the cluster structure starts to change, evidenced by the splitting of the 3.6 ppm NMR peak into two weak broad peaks at 3.55 and 3.65 ppm, and the 3.8 ppm signal was also found to shift downfield and merged with the peak at 4.0 ppm. These spectral changes indicate that thiolates in mode I, albeit resistant to a low dose of $Ce(SO_4)_2$ (1.5 mg, 4.5 μmol, ~12 equiv of $Au_{25}$), start to be oxidized under a high dose of $Ce(SO_4)_2$ (total 3.0 mg, 9 μmol, ~24 equiv of $Au_{25}$). The optical spectroscopic measurement also showed large changes to the cluster's absorption spectrum (Figure 2): those initially prominent absorption peaks, in particular, the one at 680 nm (a spin-forbidden electronic transition), disappeared and a featureless decay was observed.

Taken together, these data clearly demonstrate the oxidation resistance difference in the two types of surface thiolates; the V-shaped binding mode (II, total six ligands; see Scheme 1) located at the second $Au_{12}$ shell is much less stable and was first attacked by oxidants, while at a higher dose of oxidants, the triangular binding mode (I, 12 ligands) will be attacked, as well. It is worthy of noting that, when the oxidant is exceedingly in excess, the surface ligands will be fully oxidized to sulfonic acid (G-$SO_3H$, detected by ESI mass spectrometry), and the nanoclusters start to aggregate into large particles revealed by TEM (data not shown).

Herein we further investigate the thermal stability of the $Au_{25}(SG)_{18}$ nanoclusters. For the thermal experiment, we used dried powders of $Au_{25}(SG)_{18}$ instead of a solution sample. The experiments were performed with a TGA instrument under a programmed temperature increase to a designated temperature at a heating rate of 5 °C/min in a $N_2$ atmosphere.

The UV−vis spectra (Figure 3) show that $Au_{25}(SG)_{18}$ is stable up to ~160 °C (kept at this temperature for 2 h), evidenced by the resemblance of the spectral profile to that of the starting $Au_{25}(SG)_{18}$ nanoclusters, in which all the characteristic peaks are retained. On the other hand, NMR analysis shows quite complex behavior of the thermally treated sample. We found, even when heated at a slightly elevated temperature (45 °C) under a $N_2$ atmosphere (for 6 h), the NMR spectrum of $Au_{25}(SG)_{18}$ clusters already exhibited some changes compared with that of the original sample; that is, the 3.95 ppm (assigned as 9-C**$H_2$**) and 3.8 ppm (assigned as 2-C**H**) merged into a broad peak at ~3.85 ppm, which smeared out the nearby 3.6/3.8 ppm doublet peaks; note that the 3.6/3.8 ppm doublet is from the 12 thiolates in the triangular mode I. The two side chains of glutathionate bear −COOH groups and are hydrogen bonded, hence, they are quite sensitive to thermal treatment. The changes in the NMR signals for the 45 °C treatment should only reflect changes to the carboxyl groups and/or the amine in the −SG ligands; the Au−S linkages and the $Au_{25}$ core should not be affected. MALDI mass spectrometry analysis showed an

almost identical MALDI pattern to that of the starting material (Figure 5), indicating that no changes occurred to the core of $Au_{25}(SG)_{18}$ after thermal treatment at 45 °C, even at 145 °C. Therefore, the thermal treatment at 45 up to 145 °C only causes changes to the side chains, which affects the 2-H and 9-H NMR signals. Since such changes solely occur to the side groups of the thiolate ligands and do not affect the Au−S linkages and the $Au_{25}$ core structure, the optical properties of the clusters are retained for thermal treatment below ~160 °C (Figure 3).

When the $Au_{25}(SG)_{18}$ clusters were treated at 160 °C (for 1 h), the doublet at 3.3/3.4 ppm disappeared, indicating possible desorption of six mode II ligands (Figure 4, spectrum d). Note that the disappearance of the doublet is not because of its merging with nearby peaks; indeed, extra sharp peaks were found at 4.1, 2.3, 2.0, and ~1.4 ppm, which should arise from the desorbed glutathione-related compound. Further heating for another hour at 160 °C does not lead to further changes in NMR spectra (Figure 4, spectrum e), which indicates that the intermediate product is quite stable at 160 °C.

When the $Au_{25}(SG)_{18}$ clusters were treated at 180 °C, dramatic changes in the NMR spectrum occurred (Figure 4, spectrum f). The original NMR peaks were almost completely lost, and many new sharp peaks became prominent, indicating that the −SG ligand shell starts to collapse, but no mass loss was found at this temperature, evidenced by the TGA analysis. In the UV−vis spectra, the characteristic peaks for $Au_{25}(SG)_{18}$ also disappeared at 180 °C and a featureless decay curve was observed (Figure 3). By comparing the NMR peak areas at 1.99, 2.36, and 4.13 ppm (Figure 4, spectra e and f), we estimated the ratio of dissociated ligands at 160 °C to those at 180 °C to be roughly 1:2. This again indicates that the six mode II ligands were first dissociated at ~160 °C (Figure 3, spectra e), followed by the 12 model I ligands at ~180 °C. Since the optical properties of $Au_{25}(SG)_{18}$ are primarily contributed by the $Au_{13}$ kernel rather than by the exterior shell of 12 gold atoms, the thermal desorption of the six mode II thiolates at 160 °C does not affect the optical spectrum (Figure 3). Only when the mode I ligands were desorbed at 180 °C did the optical spectrum start to collapse.

Taken together, both the oxidation and thermal experiments explicitly demonstrate the distinct stability differences for the two binding modes of surface thiolate ligands. In both processes, the triangular binding mode I seems more stable than the V-shaped mode II (Scheme 1B); the six mode II ligands are first attacked by oxidants or also first desorbed when thermally treated at 160 °C. Interestingly, the LDI-MS spectra of $Au_{25}(SG)_{18}$ showed a most abundant peak at 5314 (Figure 5), corresponding to the $[Au_{25}S_{12}]^-$ species (5308 Da, note that the 6 Da deviation from the theoretical mass of $Au_{25}S_{12}$ is caused by the default mass calibration; *in situ*

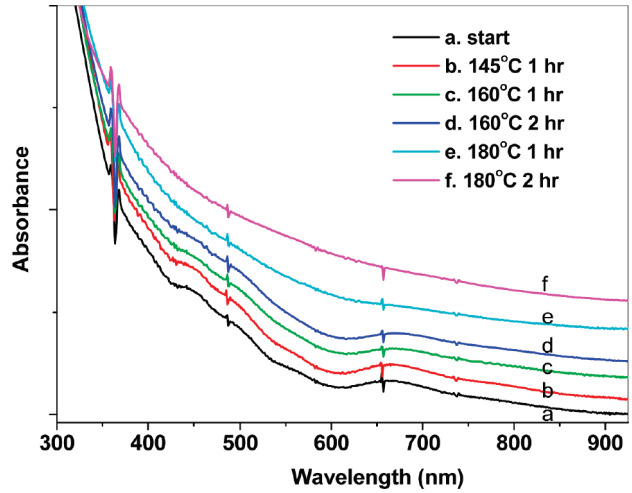


**Figure 3. UV−vis absorption spectra of $Au_{25}(SG)_{18}$ after thermal treatment at different temperatures (powders redissolved in $H_2O$ for UV−vis spectral measurements). The spectra are shifted for the ease of comparison.**

calibration was not done). This observation is consistent with the oxidation and thermal stabilities of the two Au−S binding modes in the $Au_{25}$ nanocluster; that is, the six mode II ligands are first dissociated under laser excitation in LDI-MS analysis.

Previous theoretical calculations by density functional theory[55−57] reveal an interesting electron distribution in the $Au_{25}$ core: the $Au_{13}$ kernel seems to hold eight valence electrons (but highly delocalized among the 13 atoms in the $Au_{13}$ kernel), that is, $1S^21P^6$ in the superatom picture; in contrast, the $Au_{12}$ shell (*i.e.*, the second shell) forms strong covalent bonds with thiolates, but mode I and mode II thiolates show some distinct differences. Compared with the free thiol (H-SG) in which electron transfer from H to S occurs to a significant extent, NMR also indicates similar electron

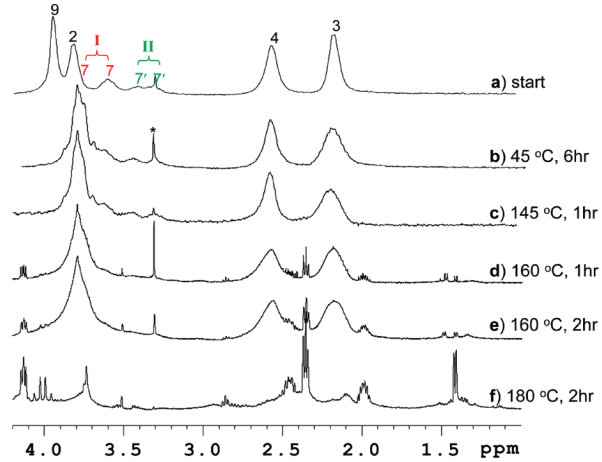


**Figure 4. NMR spectra of $Au_{25}(SG)_{18}$ after thermal treatment at different temperatures (powders redissolved in $D_2O$ for NMR measurements). The *sharp* peak at 3.3 ppm marked by an asterisk (*) arises from residual $CH_3OH$ in the $Au_{25}(SG)_{18}$ samples.**

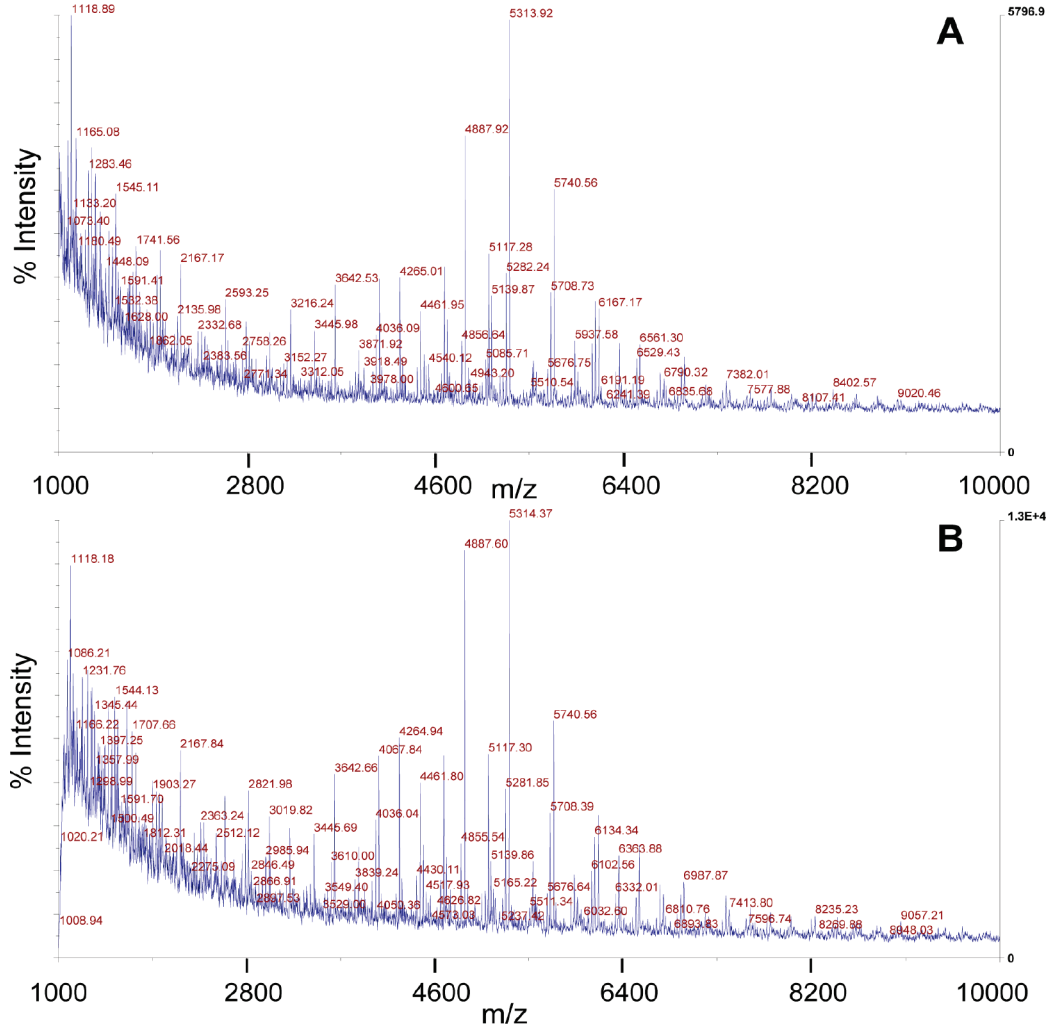


**Figure 5. MALDI mass spectra of $Au_{25}(SG)_{18}$, (A) starting material and (B) after thermal treatment at 45 °C. The peak at *m/z* 5314 is assigned to $[Au_{25}S_{12}]^-$ (theoretical mass 5308 Da, the 6 Da deviation is due to mass calibration). Spectra were acquired in the negative mode.**

transfer effect from Au to S but with different magnitudes for modes I and II; the mode I shows a larger chemical shift of α-H from 2.9 ppm (in free H-SG) to 3.6/3.8 ppm (average $\Delta\delta \sim 0.8$ ppm), while mode II shows a much smaller downfield shift from 2.9 ppm in free H-SG to 3.3/3.4 ppm in the cluster (average $\Delta\delta \sim 0.45$ ppm). These results reveal some bonding differences between $Au_{12,shell\,1}$−thiolates (mode I) and $Au_{12,shell\,2}$−thiolates (mode II); the mode II thiolates are more electron-rich compared with mode I ligands and, hence, are easier to be attacked by oxidant. The result is consistent with electron shell closing in the $Au_{13}$ kernel ($1S^21P^6$), that is to say, the electron transfer from the $Au_{13}$ kernel to S in mode I thiolates is more difficult and, hence, has less electron density on mode I thiolates compared with mode II thiolates. Upon the basis of the observations in the oxidation and the thermal experiments as well as the most abundant $[Au_{25}S_{12}]^-$ species detected in laser desorption ionization (LDI) mass spectrometry analysis of $Au_{25}(SG)_{18}$, a metastable species similar to $Au_{25}(SG)_{12}$ (*i.e.*, a loss of six mode II ligands) perhaps exist in the processes of oxidation and thermal treatment.

## CONCLUSION

In summary, this work provides an important insight into the stability differences of the two Au−S binding modes in $Au_{25}(SG)_{18}$. Specifically, our data explicitly reveal that the triangular gold−thiolate binding mode (I) is more stable than the V-shaped binding mode (II). On the basis of the stable fragment of $[Au_{25}S_{12}]^-$ observed in the LDI-MS laser-induced ionization process, as well as on the evidence from NMR and optical spectroscopic analyses, we believe that a metastable intermediate close to $Au_{25}(SG)_{12}$ may exist in the oxidation and thermal processes. Overall, the conclusions from this work help in understanding the interesting structure of $Au_{25}(SR)_{18}$ nanoclusters and provide useful information for their future potential applications such as catalysis.

## EXPERIMENTAL SECTION

**Chemicals.** Tetrachloroauric(III) acid ($HAuCl_4 \cdot 3H_2O$, >99.99% metals basis, Aldrich), L-glutathione, reduced (≥99%, Aldrich), methanol (HPLC, ≥99.9%, Aldrich), tetrahydrofuran (HPLC grade, ≥99.9%, Aldrich), and deuterium oxide (99.8 atom % D, Acros) were used. All chemicals were used as received, except THF was bubbled by $N_2$. Nanopure water (resistivity = 18.2 MΩ · cm) was produced with a Barnstead NANOpure DIwater system. All glassware was thoroughly cleaned with aqua regia ($HCl/HNO_3$ = 3:1 vol %), rinsed with copious Nanopure water, and then dried in oven prior to use.

**Synthesis of $Au_{25}$ Clusters.** For the details of synthesis $Au_{25}(SG)_{18}$, see refs 51 and 52. In the oxidation experiment, $Ce(SO_4)_2$ was used to oxidized $Au_{25}(SG)_{18}$ (in $D_2O$); the reaction was monitored by both NMR and UV−vis spectroscopy. Thermal stability of $Au_{25}(SG)_{18}$ clusters was investigated on a TG/DTA 6300 analyzer (Seiko Instruments) under a programmed temperature rise (5 °C/min) to various temperatures (see main text) in a $N_2$ atmosphere.

**Characterization.** All UV−vis absorption spectra were recorded in the range of 190−1100 nm using a Hewlett-Packard (HP) 8543 diode array spectrophotometer; mass spectrometry analyses were performed by laser desorption ionization (without matrix, LDI) and electrospray ionization (ESI); nuclear magnetic resonance (NMR) analysis was conducted on a Bruker AM 300 MHz spectrometer. Transmission electron microscopy (TEM) images were obtained using a Hitachi 7000 TEM operated at 75 kV.

*Acknowledgment.* This work is supported by CMU startup, AFOSR, and NIOSH.

## REFERENCES AND NOTES


1. Zhu, M.; Aikens, C. M.; Hollander, F. J.; Schatz, G. C.; Jin, R. Correlating the Crystal Structure of a Thiol-Protected $Au_{25}$ Cluster and Optical Properties. *J. Am. Chem. Soc.* **2008**, *130*, 5883–5885.
2. Wyrwas, R. B.; Alvarez, M. M.; Khoury, J. T.; Price, R. C.; Schaaff, T. G.; Whetten, R. L. The Colors of Nanometric Gold. *Eur. Phys. J. D* **2007**, *43*, 91–95.
3. Shichibu, Y.; Negishi, Y.; Watanabe, T.; Chaki, N. K.; Kawaguchi, H.; Tsukuda, T. Biicosahedral Gold Clusters $[Au_{25}(PPh_3)_{10}(SC_nH_{2n+1})_5Cl_2]^{2+}$ ($n$ = 2−18): A Stepping Stone to Cluster-Assembled Materials. *J. Phys. Chem. C* **2007**, *111*, 7845–7847.
4. Zhu, M.; Aikens, C. M.; Hendrich, M. P.; Gupta, R.; Qian, H.; Schatz, G. C.; Jin, R. Reversible Switching of Magnetism in Thiolate-Protected $Au_{25}$ Superatoms. *J. Am. Chem. Soc.* **2009**, *131*, 2490–2492.
5. Huang, W.; Bulusu, S.; Pal, R.; Zeng, X. C.; Wang, L.-S. Structural Transition of Gold Nanoclusters: From the Golden Cage to the Golden Pyramid. *ACS Nano* **2009**, *3*, 1225–1230.
6. Wang, G.; Huang, T.; Murray, R. W.; Menard, L.; Nuzzo, R. G. Near-IR Luminescence of Monolayer-Protected Metal Clusters. *J. Am. Chem. Soc.* **2005**, *127*, 812–813.
7. Zheng, J.; Petty, J. T.; Dickson, R. M. High Quantum Yield Blue Emission from Water-Soluble $Au_8$ Nanodots. *J. Am. Chem. Soc.* **2003**, *125*, 7780–7781.
8. Bigioni, T. P.; Whetten, R. L.; Dag, Ö. Near-Infrared Luminescence from Small Gold Nanocrystals. *J. Phys. Chem. B* **2000**, *104*, 6983–6986.
9. Wu, S.; Zeng, H.; Schelly, Z. A. Growth of Uncapped, Subnanometer Size Gold Clusters Prepared *via* Electroporation of Vesicles. *J. Phys. Chem. B* **2005**, *109*, 18715–18718.
10. Sakamoto, M; Tachikawa, T.; Fujitsuka, M.; Majima, T. Photoreactivity of As-Fabricated Au Clusters at the Single-Cluster Level. *J. Am. Chem. Soc.* **2009**, *131*, 6–7.
11. Bao, Y.; Zhong, C.; Vu, D. M.; Temirov, J. P.; Dyer, R. B.; Martinez, J. S. Nanoparticle-Free Synthesis of Fluorescent Gold Nanoclusters at Physiological Temperature. *J. Phys. Chem. C* **2007**, *111*, 12194–12198.
12. Lin, C.-A. J.; Yang, T.-Y.; Lee, C.-H.; Huang, S. H.; Sperling, R. A.; Zanella, M.; Li, J. K.; Shen, J.-L.; Wang, H.-H.; Yeh, H.-I.; Parak, W. J.; Chang, W. H. Synthesis, Characterization, and Bioconjugation of Fluorescent Gold Nanoclusters toward Biological Labeling Applications. *ACS Nano* **2009**, *3*, 395–401.
13. Liu, X.; Li, C.; Xu, J.; Lv, J.; Zhu, M.; Guo, Y.; Cui, S.; Liu, H.; Wang, S.; Li, Y. Surfactant-Free Synthesis and Functionalization of Highly Fluorescent Gold Quantum Dots. *J. Phys. Chem. C* **2008**, *112*, 10778–10783.
14. Chen, S. W.; Ingram, R. S.; Hostetler, M. J.; Pietron, J. J.; Murray, R. W.; Schaaff, T. G.; Khoury, J. T.; Alvarez, M. M.; Whetten, R. L. Gold Nanoelectrodes of Varied Size: Transition to Molecule-like Charging. *Science* **1998**, *280*, 2098–2101.
15. Ingram, R. S.; Hostetler, M. J.; Murray, R. W.; Schaaff, T. G.; Khoury, J. T.; Whetten, R. L.; Bigioni, T. P.; Guthrie, D. K.; First, P. N. 28 kDa Alkanethiolate-Protected Au Clusters Give Analogous Solution Electrochemistry and STM Coulomb Staircases. *J. Am. Chem. Soc.* **1997**, *119*, 9279–9280.
16. Georganopoulou, D. G.; Mirkin, M. V.; Murray, R. W. SECM Measurement of the Fast Electron Transfer Dynamics between $Au_{38}^{1+}$ Nanoparticles and Aqueous Redox Species at a Liquid/Liquid Interface. *Nano Lett.* **2004**, *4*, 1763–1767.
17. Yang, Y.; Chen, S. Surface Manipulation of the Electronic Energy of Subnanometer-Sized Gold Clusters: An Electrochemical and Spectroscopic Investigation. *Nano Lett.* **2003**, *3*, 75–79.
18. Quinn, B. M.; Liljeroth, P.; Ruiz, V.; Laaksonen, T.; Kontturi, K. Electrochemical Resolution of 15 Oxidation States for Monolayer Protected Gold Nanoparticles. *J. Am. Chem. Soc.* **2003**, *125*, 6644–6645.
19. Antonello, S.; Holm, A. H.; Instuli, E.; Maran, F. Molecular Electron-Transfer Properties of $Au_{38}$ Clusters. *J. Am. Chem. Soc.* **2007**, *129*, 9836–9837.
20. Garca-Raya, D.; Madueo, R.; Blzquez, M.; Pineda, T. Electrochemistry of Molecule-like $Au_{25}$ Nanoclusters Protected by Hexanethiolate. *J. Phys. Chem. C* **2009**, *113*, 8756–8761.
21. Maye, M. M.; Luo, J.; Han, L.; Kariuki, N.; Zhong, C. J. Synthesis, Processing, Assembly and Activation of Core−Shell Structured Gold Nanoparticle Catalysts. *Gold Bull.* **2003**, *36*, 75–82.
22. Chechik, V.; Crooks, R. M. Monolayers of Thiol-Terminated Dendrimers on the Surface of Planar and Colloidal Gold. *Langmuir* **1999**, *15*, 6364–6369.
23. Long, C. G.; Gilbertson, J. D.; Vijayaraghavan, G.; Stevenson, K. J.; Pursell, C. J.; Chandler, B. D. Kinetic Evaluation of Highly Active Supported Gold Catalysts Prepared from Monolayer-Protected Clusters: An Experimental Michaelis−Menten Approach for Determining the Oxygen Binding Constant during CO Oxidation Catalysis. *J. Am. Chem. Soc.* **2008**, *130*, 10103–10115.
24. Bonomi, R.; Selvestrel, F.; Lombardo, V.; Sissi, C.; Polizzi, S.; Mancin, F.; Tonellato, U.; Scrimin, P. Phosphate Diester and DNA Hydrolysis by a Multivalent, Nanoparticle-Based Catalyst. *J. Am. Chem. Soc.* **2008**, *130*, 15744–15745.
25. Gu, T.; Whitesell, J. K.; Fox, M. A. Energy Transfer from a Surface-Bound Arene to the Gold Core in ω-Fluorenyl-Alkane-1-Thiolate Monolayer-Protected Gold Clusters. *Chem. Mater.* **2003**, *15*, 1358–1366.
26. Ramakrishna, G.; Varnavski, O.; Kim, J.; Lee, D.; Goodson, T. Quantum-Sized Gold Clusters as Efficient Two-Photon Absorbers. *J. Am. Chem. Soc.* **2008**, *130*, 5032–5033.
27. Muhammed, M. A. H.; Shaw, A. K.; Pal, S. K.; Pradeep, T. Quantum Clusters of Gold Exhibiting FRET. *J. Phys. Chem. C* **2008**, *112*, 14324–14330.
28. Wohltjen, H.; Snow, A. W. Colloidal Metal−Insulator−Metal Ensemble Chemiresistor Sensor. *Anal. Chem.* **1998**, *70*, 2856–2859.
29. Rowe, M. P.; Plass, K. E.; Kim, K.; Kurdak, C.; Zellers, E. T.; Matzger, A. J. Single-Phase Synthesis of Functionalized Gold Nanoparticles. *Chem. Mater.* **2004**, *16*, 3513–3517.
30. Joseph, Y.; Guse, B.; Vossmeyer, T.; Yasuda, A. Gold Nanoparticle/Organic Networks as Chemiresistor Coatings:

The Effect of Film Morphology on Vapor Sensitivity. *J. Phys. Chem. C* **2008**, *112*, 12507–12514.
31. Bowman, M.-C.; Ballard, T. E.; Ackerson, C. J.; Feldheim, D. L.; Margolis, D. M.; Melander, C. Inhibition of HIV Fusion with Multivalent Gold Nanoparticles. *J. Am. Chem. Soc.* **2008**, *130*, 6896–6897.
32. Ackerson, C. J.; Jadzinsky, P. D.; Jensen, G. J.; Kornberg, R. D. Rigid, Specific, and Discrete Gold Nanoparticle/Antibody Conjugates. *J. Am. Chem. Soc.* **2006**, *128*, 2635–2640.
33. Zhu, M.; Qian, H.; Jin, R. Thiolate-Protected $Au_{20}$ Clusters with a Large Energy Gap of 2.1 eV. *J. Am. Chem. Soc.* **2009**, *131*, 7220–7221.
34. Schaaff, T. G.; Shafigullin, M. N.; Khoury, J. T.; Vezmar, I.; Whetten, R. L.; Cullen, W. G.; First, P. N.; Gutierrez-Wing, C.; Ascensio, J.; Jose-Yacaman, M. J. Isolation of Smaller Nanocrystal Au Molecules: Robust Quantum Effects in Optical Spectra. *J. Phys. Chem. B* **1997**, *101*, 7885–7891.
35. Tsunoyama, H.; Nickut, P.; Negishi, Y.; Al-Shamery, K.; Matsumoto, Y.; Tsukuda, T. Formation of Alkanethiolate-Protected Gold Clusters with Unprecedented Core Sizes in the Thiolation of Polymer-Stabilized Gold Clusters. *J. Phys. Chem. C* **2007**, *111*, 4153–4158. Woehrle, G. H.; Warner, M. G.; Hutchison, J. E. Ligand Exchange Reactions Yield Subnanometer, Thiol-Stabilized Gold Particles with Defined Optical Transitions. *J. Phys. Chem. B* **2002**, *106*, 9979–9981.
36. Balasubramanian, R.; Guo, R.; Mills, A. J.; Murray, R. W. Reaction of $Au_{55}(PPh_3)_{12}Cl_6$ with Thiols Yields Thiolate Monolayer Protected $Au_{75}$ Clusters. *J. Am. Chem. Soc.* **2005**, *127*, 8126–8132. Toikkanen, O.; Ruiz, V.; Ronholm, G.; Kalkkinen, N.; Liljeroth, P.; Quinn, B. M. Synthesis and Stability of Monolayer-Protected $Au_{38}$ Clusters. *J. Am. Chem. Soc.* **2008**, *130*, 11049–11055.
37. Gautier, C.; Burgi, T. Chiral Inversion of Gold Nanoparticles. *J. Am. Chem. Soc.* **2008**, *130*, 7077–7084.
38. Hussain, I.; Graham, S.; Wang, Z.; Tan, B.; Sherrington, D. C.; Rannard, S. P.; Cooper, A. I.; Brust, M. Size-Controlled Synthesis of Near-Monodisperse Gold Nanoparticles in the 1−4 nm Range Using Polymeric Stabilizers. *J. Am. Chem. Soc.* **2005**, *127*, 16398–16399.
39. Gies, A. P.; Hercules, D. M.; Gerdon, A. E.; Cliffel, D. E. Electrospray Mass Spectrometry Study of Tiopronin Monolayer-Protected Gold Nanoclusters. *J. Am. Chem. Soc.* **2007**, *129*, 1095–1104.
40. Kim, J.; Lema, K.; Ukaigwe, M.; Lee, D. Facile Preparative Route to Alkanethiolate-Coated $Au_{38}$ Nanoparticles: Postsynthesis Core Size Evolution. *Langmuir* **2007**, *23*, 7853–7858.
41. Yao, H.; Miki, K.; Nishida, N.; Sasaki, A.; Kimura, K. Large Optical Activity of Gold Nanocluster Enantiomers Induced by a Pair of Optically Active Penicillamines. *J. Am. Chem. Soc.* **2005**, *127*, 15536–15543.
42. Cathcart, N.; Mistry, P.; Makra, C.; Pietrobon, B.; Coombs, N.; Jelokhani-Niaraki, M.; Kitaev, V. Chiral Thiol-Stabilized Silver Nanoclusters with Well-Resolved Optical Transitions Synthesized by a Facile Etching Procedure in Aqueous Solutions. *Langmuir* **2009**, *25*, 5840–5846.
43. Zhang, Y.; Shuang, S.; Dong, C.; Lo, C. K.; Paau, M. C.; Choi, M. M. F. Application of HPLC and MALDI-TOF MS for Studying As-Synthesized Ligand-Protected Gold Nanoclusters Products. *Anal. Chem.* **2009**, *81*, 1676–1685.
44. Xie, J.; Zheng, Y; Ying, J. Y. Protein-Directed Synthesis of Highly Fluorescent Gold Nanoclusters. *J. Am. Chem. Soc.* **2009**, *131*, 888–889.
45. Qian, H.; Zhu, M.; Andersen, U. N.; Jin, R. Facile, Large-Scale Synthesis of Dodecanethiol-Stabilized $Au_{38}$ Clusters. *J. Phys. Chem. A* **2009**, *113*, 4281–4284.
46. Negishi, Y.; Chaki, N. K.; Shichibu, Y.; Whetten, R. L.; Tsukuda, T. Origin of Magic Stability of Thiolated Gold Clusters: A Case Study on $Au_{25}(SC_6H_{13})_{18}$. *J. Am. Chem. Soc.* **2007**, *129*, 11322–11323.
47. Tracy, J. B.; Kalyuzhny, G.; Crowe, M. C.; Balasubramanian, R.; Choi, J.-P.; Murray, R. W. Poly(ethylene glycol) Ligands for High-Resolution Nanoparticle Mass Spectrometry. *J. Am. Chem. Soc.* **2007**, *129*, 6706–6707.
48. Schaaff, T. G.; Knight, G.; Shafigullin, M. N.; Borkman, R. F.; Whetten, R. L. Isolation and Selected Properties of a 10.4 kDa Gold:Glutathione Cluster Compound. *J. Phys. Chem. B* **1998**, *102*, 10643–10646.
49. Zhu, M.; Lanni, E.; Garg, N.; Bier, Mark, E.; Jin, R. Kinetically Controlled, High-Yield Synthesis of $Au_{25}$ Clusters. *J. Am. Chem. Soc.* **2008**, *130*, 1138–1139.
50. Shichibu, Y.; Negishi, Y.; Tsunoyama, H.; Kanehara, M.; Teranishi, T.; Tsukuda, T. Extremely High Stability of Glutathionate-Protected $Au_{25}$ Clusters Against Core Etching. *Small* **2007**, *3*, 835–839.
51. Wu, Z.; Suhan, J.; Jin, R. One-pot Synthesis of Atomically Monodisperse, Thiol-Functionalized $Au_{25}$ Nanoclusters. *J. Mater. Chem.* **2009**, *19*, 622–626.
52. Wu, Z.; Gayathri, C.; Gil, R. R.; Jin, R. Probing the Structure and Charge State of Glutathione-Capped $Au_{25}(SG)_{18}$ Clusters by NMR and Mass Spectrometry. *J. Am. Chem. Soc.* **2009**, *131*, 6535–6542.
53. Zhu, M.; Eckenhoff, W. T.; Pintauer, T.; Jin, R. Conversion of Anionic $[Au_{25}(SCH_2CH_2Ph)_{18}]^-$ Cluster to Charge Neutral Cluster *via* Air Oxidation. *J. Phys. Chem. C* **2008**, *112*, 14221–14224.
54. Heaven, M. W.; Dass, A.; White, P. S.; Holt, K. M.; Murray, R. W. Crystal Structure of the Gold Nanoparticle $[N(C_8H_{17})_4][Au_{25}(SCH_2CH_2Ph)_{18}]$. *J. Am. Chem. Soc.* **2008**, *130*, 3754–3755.
55. Akola, J.; Walter, M.; Whetten, R. L.; Häkkinen, H.; Grönbeck, H. On the Structure of Thiolate-Protected $Au_{25}$. *J. Am. Chem. Soc.* **2008**, *130*, 3756–3757.
56. Aikens, C. M. Origin of Discrete Optical Absorption Spectra of $M_{25}(SH)_{18}^-$ Nanoparticles (M = Au, Ag). *J. Phys. Chem. C* **2008**, *112*, 19797–19800.
57. Jiang, D.-e.; Dai, S. From Superatomic $Au_{25}(SR)_{18}^-$ to Superatomic $M@Au_{24}(SR)_{18}^q$ Core−Shell Clusters. *Inorg. Chem.* **2009**, *48*, 2720–2722.